Inorg. Chem. **2008**, *47*, 7083−7093

Catechol Oxidase Activity of a Series of New Dinuclear Copper(II) Complexes with 3,5-DTBC and TCC as Substrates: Syntheses, X-ray Crystal Structures, Spectroscopic Characterization of the Adducts and Kinetic Studies

Kazi Sabnam Banu,[†] Tanmay Chattopadhyay,[†] Arpita Banerjee,[†] Santanu Bhattacharya,[‡] Eringathodi Suresh,[§] Munirathinam Nethaji,[||] Ennio Zangrando,*[,⊥] and Debasis Das*[,†]

Department of Chemistry, University of Calcutta, 92, A. P. C. Road, Kolkata −700 009, India, Department of Chemistry, Maharaja Manindra Chandra College, Kolkata - 700 003, India, Analytical Science Discipline, Central Salt and Marine Chemicals Research Institute, G. B. Marg, Bhavnagar-364 002, India, Department of Inorganic and Physical Chemistry, Indian Institute of Science, Bangalore- 560 012, India, and Dipartimento di Scienze Chimiche, University of Trieste, Via L. Giorgieri 1, 34127 Trieste, Italy

Received July 5, 2007

A series of dinuclear copper(II) complexes has been synthesized with the aim to investigate their applicability as potential structure and function models for the active site of catechol oxidase enzyme. They have been characterized by routine physicochemical techniques as well as by X-ray single-crystal structure analysis: $[Cu_2(H_2L2^2)(OH)(H_2O)(NO_3)](NO_3)_3 \cdot 2H_2O$ (**1**), $[Cu(HL1^4)(H_2O)(NO_3)]_2(NO_3)_2 \cdot 2H_2O$ (**2**), $[Cu(L1^1)(H_2O)(NO_3)]_2$ (**3**), $[Cu_2(L2^3)(OH)(H_2O)_2](NO_3)_2$, (**4**) and $[Cu_2(L2^1)(N_3)_3]$ (**5**) [L1 = 2-formyl-4-methyl-6R-iminomethyl-phenolato and L2 = 2,6-bis(R-iminomethyl)-4-methyl-phenolato; for $L1^1$ and $L2^1$, R = *N*-propylmorpholine; for $L2^2$, R = *N*-ethylpiperazine; for $L2^3$, R = *N*-ethylpyrrolidine, and for $L1^4$, R = *N*-ethylmorpholine]. Dinuclear **1** and **4** possess two "end-off" compartmental ligands with exogenous μ-hydroxido and endogenous μ-phenoxido groups leading to intermetallic distances of 2.9794(15) and 2.9435(9) Å, respectively; **2** and **3** are formed by two tridentate compartmental ligands where the copper centers are connected by endogenous phenoxido bridges with Cu−Cu separations of 3.0213(13) and 3.0152(15) Å, respectively; **5** is built by an end-off compartmental ligand having exogenous μ-azido and endogenous μ-phenoxido groups with a Cu−Cu distance of 3.133(2) Å (mean of two independent molecules). The catecholase activity of all of the complexes has been investigated in acetonitrile and methanol medium by UV−vis spectrophotometric study using 3,5-di-*tert*-butylcatechol (3,5-DTBC) and tetrachlorocatechol (TCC) as substrates. In acetonitrile medium, the conversion of 3,5-DTBC to 3,5-di-*tert*-butylbenzoquinone (3,5-DTBQ) catalyzed by **1**−**5** is observed to proceed via the formation of two enzyme−substrate adducts, ES1 and ES2, detected spectroscopically for the first time. In methanol medium no such enzyme−substrate adduct has been detected, and the 3,5-DTBC to 3,5-DTBQ conversion is observed to be catalyzed by **1**−**5** very efficiently. The substrate TCC forms an adduct with **2**−**5** without performing further oxidation to TCQ due to the high reduction potential of TCC (in comparison with 3,5-DTBC). But most interestingly, **1** is observed to be effective even in TCC oxidation, a process never reported earlier. Kinetic experiments have been performed to determine initial rate of reactions (3,5-DTBC as substrate, in methanol medium) and the activity sequence is **1** > **5** > **2** = **4** > **3**. A treatment on the basis of Michaelis−Menten model has been applied for kinetic study, suggesting that all five complexes exhibit very high turnover number, especially **1**, which exhibits turnover number or K_{cat} of 3.24×10^4 (h^{-1}), which is ∼3.5 times higher than the most efficient catalyst reported to date for catecholase activity in methanol medium.

Introduction

Catechol oxidase (CO), known officially as 1,2-benzenediol/oxygen oxidoreductase, is a less well-known member of type III copper proteins.[1] It is also familiar as *o*-diphenol oxidase as it catalyzes exclusively the oxidation of catechols (i.e., *o*-diphenols) to the corresponding quinones, a process known as catecholase activity (Scheme 1), and for this peculiar ability COs may take key role as disease resistant

* To whom correspondence should be addressed. E-mail: dasdebasis2001@yahoo.com (D.D.).
[†] University of Calcutta.
[‡] Maharaja Manindra Chandra College.
[§] Central Salt and Marine Chemicals Research Institute.
[||] Indian Institute of Science.
[⊥] University of Trieste.

10.1021/ic701332w CCC: $40.75
Published on Web 07/15/2008

in higher plants. Quinones are highly reactive compounds, which undergo autopolymerization to produce melanin, a brown pigment, and this process is most likely responsible to protect the damaged tissues against pathogens and insects.

Tyrosinase (TYR) represents another type III copper enzyme that may also promote catechol oxidation with additional capability to show cresolase activity, thus accepting monophenol as a substrate. COs are generally found in plant tissues and in some insects and crustaceans,[2] whereas TYRs can be obtained from a variety of plants, fungi, bacteria, mammalians, and insects.[1,2] The functional differences between CO and TYR are not very rigorous because some plant COs also exhibit weak monooxygenase activity. However, they manifest some common peculiar features such as antiferromagnetism, EPR inactivity in the met state, transfer of two or more electrons reversibly and simultaneously at positive potentials, and so forth. On the other hand, CO cannot act on tyrosine as substrate.[3,4] The X-ray structural determination of CO from sweet potatoes *Ipomoea batatas* (*IbCO*),[5] in different forms, gives us an ample opportunity to investigate the structure−function relationship and to get deep insight about the functional mechanism for developing ultimately accurate structural functional models of the native enzymes. In the met form, the two copper (II) ions, at a distance of 2.9 Å, are bridged by a hydroxide ion, and each metal is further coordinated by three histidine residues. In deoxy state, a different coordination number is exhibited by the two copper(I) centers, being one four-coordinated (an aqua and three histidine ligands), the other three-coordinated (all are histidine ligands), and the two Cu(I) ions are separated by 4.4 Å. The blue-colored oxy state of CO, obtained after dioxygen binding, exhibits characteristic absorption maxima at 343 and 580 nm assigned to an O_2^{2-} (π_σ^*) → Cu(II) (ε = 6500 cm^{-1} M^{-1}) and O_2^{2-} (π_σ^*) → Cu(II) (ε = 450 cm^{-1} M^{-1}) charge-transfer transition, respectively (both extinction coefficients pertain to the copper atoms of IbCO[5]). A model study with dinuclear copper(II) complexes has received a great deal of attention.[6−24] Tremendous efforts are still underway to know the structure−function relations by tuning several parameters such as

Scheme 1

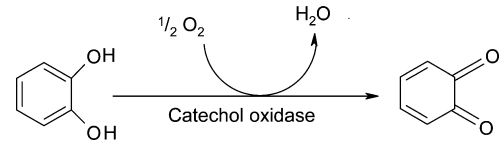

electronic and steric factors around the copper coordination spheres, copper−copper distance, number and nature of donor sites, flexibility of the donor and bridging ligands, and so forth, to understand the mechanism as well as to synthesize true structure−functional models of CO. The numerous model compounds reported so far achieve catechol oxidase activity (against a common substrate, 3,5-di-*tert*-butylcatechol), which is several thousand folds slower than the native enzymes.[25] To the best of our knowledge the most active catalyst reported so far exhibits a turnover number or K_{cat} of 9927 h^{-1}, [20] whereas the value for catechol oxidase from sweet potatoes is 8254.8 × 10^3 h^{-1}, toward catechol. Moreover, in spite of extensive studies on the mechanism of CO, most are speculative, and several important questions are still unanswered,[1,26,27] in particular the coordination mode of the substrate. The formation of an enzyme−substrate adduct has been properly proposed, but to date experimental

(1) (a) Solomon, E. I.; Sundaram, U. M.; Machonkin, T. E. *Chem.Rev* **1996**, *96*, 2563. (b) Gerdemann, C.; Eicken, C.; Krebs, B. *Acc. Chem. Res.* **2002**, *35*, 183. (c) Koval, I. A.; Gamez, P.; Belle, C.; Selmeczib, K.; Reedijk *J. Chem. Soc. Rev.* **2006**, *35*, 814.

(2) Hughes, A. L. *Immunogenetics* **1999**, *49*, 106 Evolution of the arthropod prophenoloxidase/hexamerin protein family.

(3) Mayer, A. M.; Harel, E. *Phytochemistry* **1979**, *18*, 193 Polyphenol oxidases in plants.

(4) Walker, J. R.; Ferrar, P. H. *Biotechnol. Genet. Eng. Rev.* **1998**, *15*, 457 Diphenol oxidases, enzyme-catalyzed browning and plant disease resistance.

(5) Klabunde, T.; Eicken, C.; Sacchettini, J. C.; Krebs, B. *Nat. Struct. Biol.* **1998**, *5*, 1084.

(6) (a) Reim, J.; Krebs, B. *J. Chem. Soc., Dalton Trans.* **1997**, 3793. (b) Eicken, C.; Zippel, F.; Buldt-Karentzopoulos, K.; Krebs, B. *FEBS Lett.* **1998**, *436*, 293. (c) Than, R.; Feldmann, A. A.; Krebs, B. *Coord. Chem. Rev.* **1999**, *182*, 211. (d) Gentschev, P.; Moller, N.; Krebs, B. *Inorg. Chim. Acta* **2000**, *300*, 442. (e) Merkel, M.; Mçller, N.; Piacenza, M.; Grimme, S.; Rompel, A.; Krebs, B *Chem.−Eur. J.* **2005**, *11*, 1201.

(7) Monzani, E.; Quinti, L.; Perotti, A.; Casella, L.; Gullotti, M.; Randaccio, L.; Geremia, S.; Nardin, G.; Faleschini, P.; Tabbi, G. *Inorg. Chem.* **1998**, *37*, 553.

(8) Manzur, J.; Garcia, A. M.; Vega, A.; Spodine, E. *Polyhedron* **1999**, *18*, 2399.

(9) (a) Torelli, S.; Belle, C.; Gautier-; Luneau, I.; Pierre, J. L.; Saint- Aman, E.; Latour, J. M.; Le Pape, L.; Luneau, D. *Inorg. Chem.* **2000**, *39*, 3526. (b) Torelli, S.; Belle, C.; Hamman, S.; Pierre, J.-L. *Inorg. Chem.* **2002**, *41*, 3983. (c) Belle, C; Selmeczi, K; Torelli, S; Pierre, J-L; *C. R. Chimie* **2007**, *10*, 271.

(10) Gupta, M.; Mathur, P.; Butcher, R. J. *Inorg. Chem.* **2001**, *40*, 878.

(11) Murthy, N. N.; Mahroof-Tahir, M.; Karlin, K. D. *Inorg. Chem.* **2001**, *40*, 628.

(12) Kao, C. H.; Wei, H. H.; Liu, Y. H.; Lee, G. H.; Wang, Y.; Lee, C. J. *J. Inorg. Biochem.* **2001**, *84*, 171.

(13) Fernandes, C.; Neves, A.; Bortoluzzi, A. J.; Mangrich, A. S.; Rentschler, E.; Szpoganicz, B.; Schwingel, E. *Inorg. Chim. Acta* **2001**, *320*, 12.

(14) Mukherjee, J.; Mukherjee, R. *Inorg. Chim. Acta* **2002**, *337*, 429.

(15) Neves, A.; Rossi, L. M.; Bortoluzzi, A. J.; Szpoganicz, B.; Wiezbicki, C.; Schwingel, E.; Haase, W.; Ostrovsky, S. *Inorg. Chem.* **2002**, *41*, 1788.

(16) (a) Ackermann, J.; Meyer, F.; Kaifer, E.; Pritzkow, H. *Chem. Eur. J.* **2002**, *8*, 247. (b) Ackermann, J; Buchler, S; Meyer, F *C. R. Chimie* **2007**, *10*, 421.

(17) Seneque, O.; Campion, M.; Douziech, B.; Giorgi, M.; Riviere, E.; Journaux, Y.; Mest, Y. L.; Reinaud, O. *Eur. J. Inorg. Chem.* **2002**, 2007.

(18) (a) Koval, I. A.; Pursche, D.; Stassen, A. F.; Gamez, P.; Krebs, B.; Reedjik, J. *Eur. J. Inorg. Chem.* **2003**, 1669. (b) Koval, I. A.; Huisman, M.; Stassen, A. F.; Gamez, P.; Lutz, M.; Spek, A. L.; Reedijk, J. *Eur. J. Inorg. Chem.* **2004**, 591. (c) Koval, I. A.; Belle, C.; Selmeczi, K.; Philouze, C.; Eric, S. A.; Schuitema, A. M.; Gamez, P.; Pierre, J. L.; Reedjik, J. *J. Biol. Inorg. Chem* **2005**, *10*, 739.

(19) (a) Sreenivasulu, B.; Vetrichelvan, M.; Zhao, F.; Gao, S.; Vittal, J. J. *Eur. J. Inorg. Chem.* **2005**, 4635. (b) Sreenivasulu, B.; Zhao, F.; Gao, S.; Vittal, J. J. *Eur. J. Inorg. Chem.* **2006**, 2656.

(20) (a) Wegner, R.; Gottschaldt, M.; Wolfgang, P.; Jager, E.-G.; Klemm, D. *J. Mol. Catal. A* **2003**, *201*, 93.

(21) Fernandes, C.; Neves, A.; Bortoluzzi, A. J; Mangrich, A. S.; Rentschler, E.; Szpoganicz, B.; Schwingel, E. *Inorg. Chim. Acta* **2001**, *320*, 12.

(22) Thirumavalavan, M.; Akilan, P.; Kandaswamy, M.; Chinnakali, K.; Kumar, G. S.; Fun, H. K. *Inorg. Chem.* **2003**, *42*, 3308.

(23) Kaizer, J.; Csonka, R.; Speir, G.; Giorgi, M.; Reglier, M. *J. Mol. Catal. A* **2005**, *235*, 81.

(24) Lee, C. H.; Wong, S. T.; Lin, T. S.; Mou, C. Y. *J. Phys. Chem. B* **2005**, *109*, 775.

(25) Karlin, K. D.; Kaderli, S.; Zuberbühler, A. D. *Acc. Chem. Res.* **1997**, 139.

(26) Eicken, C.; Krebs, B.; Sacchettini, J. C. *Curr. Opin. Struct. Biol.* **1999**, *9*, 677.

(27) Siegbahn, P. E. M. *J. Biol. Inorg. Chem.* **2004**, *9*, 577.

Scheme 2. Structures of the End-Off Compartmental Ligands

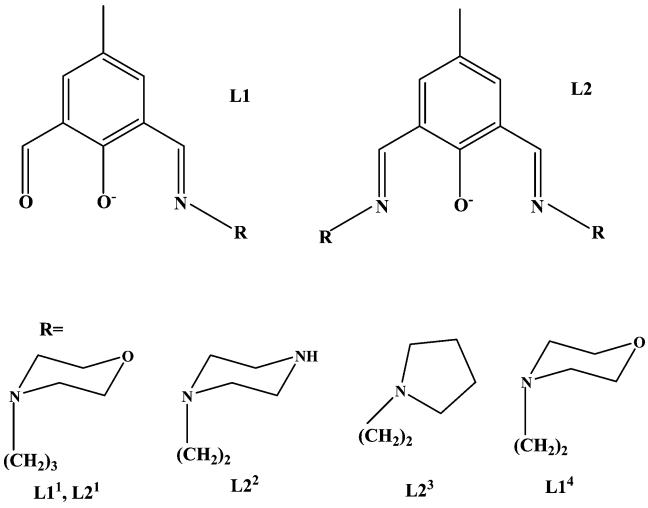

evidence have been achieved with tetrachlorocatechol as substrate,[28] which is difficult to oxidize due to its very high redox potential in contrast to 3,5-DTBC, and no direct evidence is described in the literature with the latter. For the present work, we have judiciously designed a series of compartmental ligands (end-off type) to maintain the Cu−Cu separation around 3 Å, because, as suggested by literature survey, such an intermetallic distance may generate the most efficient catalytic process. We are reporting herein the syntheses, characterization, and catecholase activity study of five new dinuclear copper(II) complexes, $[Cu_2(H_2L2^2)(OH)(H_2O)(NO_3)](NO_3)_3\cdot 2H_2O$(**1**),$[Cu(HL1^4)(H_2O)(NO_3)]_2(NO_3)_2\cdot 2H_2O$ (**2**), $[Cu(L1^1)(H_2O)(NO_3)]_2$ (**3**), $[Cu_2(L2^3)(OH)(H_2O)_2](NO_3)_2$, (**4**), and $[Cu_2(L2^1)(N_3)_3]$ (**5**) of compartmental Schiff-base ligands (Scheme 2) obtained from condensation of 4-methyl-2,6-diformylphenol with *N*-(2-aminoethyl)piperazine (aepp), *N*-(2-aminoethyl)morpholine (aemp), *N*-(3-aminopropyl)morpholine (apmp), and *N*-(2-aminoethyl)pyrrolidine (aepd) (Scheme 2). Our investigation generates not only the most efficient synthetic analogues for the active site of catechol oxidase with K_{cat} as high as 3.24×10^4 h^{-1} but also establishes spectroscopically the adduct formation between copper centers and 3,5-DTBC, thus characterizing the very first step of catecholase activity of copper(II) complexes with this substrate, and the oxidation of TCC, a novel phenomenon exhibited by synthetic analogue of catechol oxidase.

Experimental Section

General Remarks. All chemicals were obtained from commercial sources and used as received. Solvents were dried according to standard procedure and distilled prior to use. 4-methyl-2,6-diformylphenol was prepared according to the literature method.[29] *N*-(2-aminoethyl)piperazine, *N*-(2-aminoethyl)morpholine, *N*-(3-aminopropyl)morpholine, and *N*-(2-aminoethyl)pyrrolidine were purchased from Alfa Aesar Chemical Company and used as received. All other chemicals used were of AR grade.

Physical Measurements. Elemental analyses (carbon, hydrogen, and nitrogen) were performed using a PerkinElmer 240C elemental analyzer. Copper was estimated gravimetrically with α-benzoin oxime. Infrared spectra (4000−400 cm^{-1}) were recorded at 27 °C using a Shimadzu FTIR-8400S where KBr was used as medium. Electronic spectra (800−200nm) were obtained at 27 °C using a Shimadzu UV-3101PC where dry acetonitrile/dry methanol/nujol was used as a medium as well as a reference. The electrospray mass spectra were recorded on a MICROMASS Q-TOF mass spectrometer. The cyclic voltammetric measurements were carried out in dry acetonitrile solutions with 0.1 M tetraethylammonium perchlorate as supporting electrolyte employing a PAR potentiostat/galvanostat model Versa Stat-II. A three-electrode system was used in which the counter and working electrodes were platinum foils and the reference electrode was a saturated calomel electrode.

X-ray Data Collection and Crystal Structure Determinations. Diffraction data for the structures **1**−**3** were carried out on a Bruker Smart Apex CCD by using Mo Kα radiation (λ = 0.71073 Å), those of the structures **4** and **5** were performed on a Nonius DIP-1030H system (λ = 0.71073 Å). Experiments were performed at 100(2) K for **1**−**2**, at room temperature for **3**−**5**. Cell refinement, indexing and scaling of the data sets were carried out using Bruker *Smart*, Bruker *Saint*,[30] *Denzo*, and *Scalepack* programs.[31] All the structures were solved by direct methods and subsequent Fourier analyses[32] and refined by the full-matrix least-squares method based on F^2 with all observed reflections.[32] In crystal structure analysis of **1** and **3**, hydrogen atoms of water molecules and of hydroxido ligands not located on the ΔF maps; in **2** and **3** nitrate disordered over two positions with occupancies of 0.79(1)/0.21(1) and 0.717(19)/0.283(19), respectively, and atoms at lower occupancy were isotropically refined; in **2** and **4** O−H distances of water molecules were restrained at 0.9 Å. All hydrogen atoms were placed at geometrically calculated positions, except those of water molecules as indicated above. Both the *N*-2(aminopropyl)morpholine ligands in one independent molecule of **5** were found disordered over two conformations (occupancy factor of 0.5 each), and atoms of all morpholine fragments were isotropically refined due to the high thermal motion. All the calculations were performed using the *WinGX System*, version 1.70.01.[33] Crystallographic data and experimental details are reported in Table 1.

Syntheses. a. 1: $[Cu_2(H_2L2^2)(OH)(H_2O)(NO_3)](NO_3)_3\cdot 2H_2O$. A methanolic solution (5 mL) of *N*-(2-aminoethyl)piperazine (0.258 g, 2 mmol) was added dropwise to a heated methanolic solution (10 mL) of 4-methyl-2,6-diformylphenol (0.164 g, 1 mmol), and the resulting mixture was boiled for half an hour. Then, a methanolic solution (15 mL) of $Cu(NO_3)_2\cdot 3H_2O$ (0.604 g, 2.5mmol) was added and the resulting mixture refluxed for two hours. After cooling, the clear deep-green solution was kept in a $CaCl_2$ desiccator in dark, and square-shaped deep-green crystals, suitable for X-ray data collection, were obtained after a few days. (Yield 70%). Anal. Calcd for $C_{21}H_{42}N_{10}O_{17}Cu_2$ (**1**): C, 30.25; H, 5.08; N, 16.80; Cu, 15.24. Found: C, 30.29; H, 5.11; N, 16.84; Cu, 15.27%;

b. 2: $[Cu(HL1^4)(H_2O)(NO_3)]_2(NO_3)_2\cdot 2H_2O$. It was prepared similarly as for **1** by using *N*-(2-aminoethyl)morpholine (0.261 g, 2 mmol) instead of *N*-(2-aminoethyl)piperazine. (Yield 73%). Anal.

(28) (a) Börzel, H.; Comba, P.; Pritzkow, H. *Chem. Commun.* **2001**, 97. (b) Born, K; Comba, P; Daubinet, A; Fuchs, A; Wadepohl, H *J. Biol. Inorg. Chem.* **2007**, *12*, 36, and references therein.
(29) Gagne, R. R.; Spiro, C. L.; Smith, T. J.; Hamann, C. A.; Thies, W. R.; Shiemeke, A. K. *J. Am. Chem. Soc.* **1981**, *103*, 4073.
(30) *SMART, SAINT. Software Reference Manual*; Bruker AXS Inc.: Madison, Wisconsin, USA, 2000.
(31) Otwinowski Z. and, Minor, W. Processing of X-ray Diffraction Data Collected in Oscillation Mode. In *Methods in Enzymology, Methods in Enzymology*; Carter, C. W., Jr.; Sweet, R. M., Eds.; New York: Academic Press, 1997, Vol. *276*, pp −326..
(32) Sheldrick, G. M. *SHELX97 Programs for Crystal Structure Analysis (Release 97−2)*; University of Göttingen: Göttingen, Germany, 1998.
(33) Farrugia, L. J. *J. Appl. Crystallogr.* **1999**, *32*, 837.

Table 1. Crystallographic Data and Details of Refinements for **1**−**5**

	1	2	3	4	5
empirical formula	$C_{21}H_{42}Cu_2N_{10}O_{17}$	$C_{30}H_{48}Cu_2N_8O_{22}$	$C_{32}H_{46}Cu_2N_6O_{14}$	$C_{21}H_{36}Cu_2N_6O_{10}$	$C_{46}H_{70}Cu_4N_{26}O_6$
fw	833.73	999.84	865.83	659.64	1337.44
cryst syst	orthorhombic	orthorhombic	monoclinic	monoclinic	trigonal
space group	$Pna2_1$	$Pbcn$	$P2_1/c$	$P2_1/m$	R $\bar{3}$
a /Å	8.614(2)	16.365(3)	12.695(4)	8.158(2)	37.033(6)
b /Å	39.907(5)	14.434(2)	10.000(3)	12.416(3)	
c /Å	9.560(2)	16.890(3)	16.260(5)	13.622(3)	21.890(4)
β /°			99.047(6)	102.99(2)	
V /Å^3	3286.3(11)	3989.6(12)	2038.5(11)	1344.5(5)	26000(8)
Z	4	4	2	2	18
D_{calcd} /g cm^{-3}	1.685	1.665	1.411	1.629	1.538
μ /mm^{-1}	1.385	1.164	1.112	1.646	1.523
$F(000)$	1728	2072	900	684	12456
total data	21 107	25 582	9003	16 953	36 915
unique data	7202	4081	3243	3911	8283
R_{int}	0.0866	0.1139	0.0573	0.0237	0.0768
reflns $I > 2\sigma(I)$	6179	3089	2223	3125	4072
params	452	306	257	201	655
GOF	1.190	1.098	0.994	1.119	0.852
R1	0.0879	0.0781	0.0733	0.0452	0.0547
wR2 ($I > 2\sigma(I)$)[a]	0.1679	0.1649	0.1972	0.1406	0.1503
residuals /e Å^{-3}	0.782, −1.471	1.720, −0.594	1.126, −0.369	0.956, −0.892	0.754, −0.421

[a] $R1 = \Sigma||F_o| - |F_c||/\Sigma|F_o|$, $wR2 = [\Sigma w(F_o^2 - F_c^2)^2/\Sigma w(F_o^2)^2]^{1/2}$.

Calcd for $C_{30}H_{48}N_8O_{22}Cu_2$ (**2**): C, 36.04; H, 4.84; N, 11.21; Cu, 12.71. Found: C, 36.00; H, 4.83; N, 11.16; Cu, 12.76%.

c. 3: [Cu(L1^1)(H$_2$O)(NO$_3$)]$_2$. The complex was synthesized by adopting a similar procedure as for **1** by using *N*-(3-aminopropyl)morpholine (0.288 g, 2mmol) instead of *N*-(2-aminoethyl)piperazine. (Yield 67%). Anal. Calcd for $C_{32}H_{46}N_6O_{14}Cu_2$ (3): C, 44.39; H, 5.31; N, 9.71; Cu, 14.68. Found: C, 44.42; H, 5.36; N, 9.77; Cu, 14.72%.

d. 4: [Cu$_2$(L2^3)(OH)(H$_2$O)$_2$](NO$_3$)$_2$. It was prepared following a similar procedure as for **1**, using *N*-(2-aminoethyl) pyrrolidine (0.256 g, 2mmol) in place of *N*-(2-aminoethyl)piperazine. (Yield 72%). Anal. Calcd for $C_{21}H_{36}N_6O_{10}Cu_2$ (**4**): C, 38.24; H, 5.50; N, 12.74; Cu, 19.27. Found: C, 38.27; H, 5.47; N, 12.76; Cu, 19.25%.

e. 5: [Cu$_2$(L2^1)(N$_3$)$_3$]. Methanolic (10 mL) solution of sodium azide (0.325 g, 5mmol) was added dropwise to a cooled solution of **3** and stirring continuously for further 6 h. The dark green solution obtained was kept in a $CaCl_2$ desiccator in dark. After a few days cube shaped dark-green crystals of the complex were separated out. (Yield 65%). Anal. Calcd for $C_{23}H_{35}N_{13}O_3Cu_2$ (**5**): C, 41.31; H, 5.28; N, 27.23; Cu, 19.01. Found: C, 41.33; H, 5.25; N, 27.27; Cu, 19.05%.

Caution. *Azide salts are potentially explosive and should be handled with small quantities with care. No problems were faced with the complex reported herein.*

Results and Discussion

Synthesis of Dicopper(II) Complexes. 1−**4** are prepared by applying template synthesis technique by treating methanolic solution of copper(II) nitrate trihydrate with the Schiff-base formed in situ between 4-methyl-2,6-diformylphenol and the diamines (aepp, aemp, apmp, and aepd). **5** is obtained by adding excess of sodium azide [five times with respect to copper(II) nitrate salt] to **3**. The IR and UV−vis spectral data for **1**−**5** are given in Table 2. All the complexes show bands due to C═N stretch in the range 1635−1649 cm^{-1} and skeletal vibration in the range 1549−1560 cm^{-1}. Broad bands centered in the range 1375−1390 cm^{-1} are exhibited by **1**−**4** due to the weakly coordinated NO_3^- ion.[34] **5** lacks of any broadband around 1380 cm^{-1}, indicating the absence of NO_3^- ion in this complex. On the other hand, it exhibits very strong bands at 2087 and 2034 cm^{-1} corresponds to ν_{as} (azide) for bridging and terminal azide, respectively. However, we note that no well-defined criterion discriminating the coordination mode of azide (i.e., end-on or end-to-end) can be applied. The electronic spectra of **1**−**5** have been studied in the solid state (dispersed in Nujol mull) as well as in solution using CH_3CN and CH_3OH as solvents. We note that **3** exhibits low solubility in CH_3CN. The absorption bands observed in the range 622−676 nm correspond to d−d transitions, and the strong bands at 358−402 nm are caused by LMCT. Both phenoxido−Cu(II) and hydroxido−Cu(II) LMCT are observed in the region of 350−400 nm and in some cases the bands may shift to 450 nm. In case of **1**, the phenoxido−Cu(II) and hydroxido−Cu(II) LMCT bands combine to exhibit a single band. It is well-known that for a d^9 system the electronic transition $^2E_g \rightarrow {}^2T_{2g}$ is expected to take place at around 800 nm for octahedral geometry, and this band will undergo a significant blue shift on distortion of octahedral coordination to a square-pyramidal and square-

Table 2. Electronic and Infrared Spectral Data

	λ_{max}, nm ε(M^{-1}, cm^{-1})			
compound	in CH_3CN	in CH_3OH	in Nujol	IR (KBr)/cm^{-1}
1	370 (7670), 631 (249)	370 (7660), 633 (242)	365, 635	1649, 1554, 1381
2	375 (7819), 662 (631)	373 (7816), 666 (627)	373, 668	1635, 1558, 1389
3	376 (6399), 670 (87)	376 (6382), 673 (82)	370, 668	1637, 1557, 1378
4	368 (7849), 622 (216)	365 (7841), 628 (213)	370, 628	1643, 1549, 1385
5	385 (3842), 676 (166)	381 (3837), 672 (159)	392, 680	1636, 1559, 2087, 2034

(34) Nakamoto, K. *Infrared and Raman Spectra of Inorganic and Coordination Compounds* 3rd ed.; Wiley: New York, 1978.

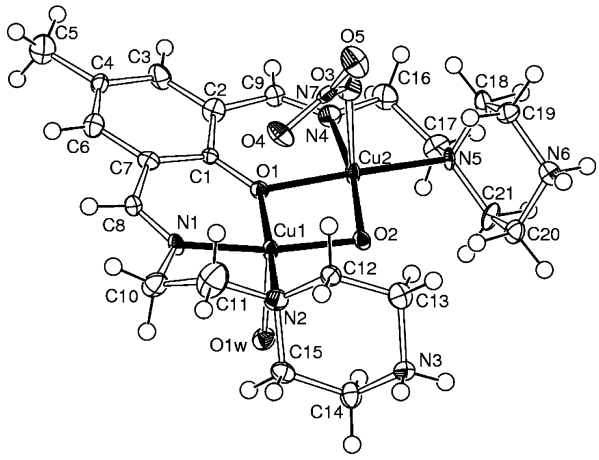

Figure 1. *ORTEP* drawing (40% probability ellipsoids) of **1** with atom labeling scheme.

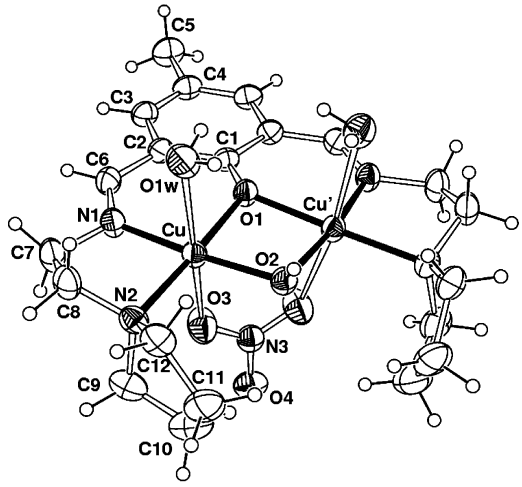

Figure 2. *ORTEP* drawing (40% probability ellipsoids) of **4** with atom labeling scheme of crystallographic independent moiety.

planar structure.[35] In **1**−**5**, the d−d transition positions are in agreement with a square-pyramidal geometry around the metal centers. Because no significant shifting in band positions is observed in solid-state electronic spectra of **1**−**5** (Table 2) when compared to the corresponding spectra recorded in solution, it may be assumed that solution and solid-state structures are very similar.

Description of Crystal Structures. (a) $[Cu_2(H_2L2^2)(OH)(H_2O)(NO_3)]\cdot(NO_3)_3\cdot 2H_2O$ (1) and $[Cu_2(L2^3)(OH)(H_2O)_2](NO_3)_2$ (4). The *ORTEP* diagram of **1** and **4** with atom number scheme is depicted in Figures 1 and 2, and a selection of bond lengths and angles are given in Table 3. Complex **4** is located on a crystallographic symmetry plane passing in between the metals and referring the two halves of the phenolato ligand. The crystal structure reveals that in both dinuclear complexes each copper atom has a distorted square-pyramidal geometry. The doubly bridging phenoxido and hydroxido oxygen atoms occupy the basal plane, and the metals complete their coordination geometry through the L2 imine- and amine-nitrogen donors from the piperazine and pyrrolidine ring in **1** and **4**, respectively. The apical positions of metal ions in complex **1** are occupied by a water molecule at Cu(1) (Cu(1)−O(1w) = 2.292(6) Å) and by a nitrate oxygen at Cu(2) (Cu(2)−O(3) = 2.404(7) Å). However, the nitrate connected to the latter metal orients a second oxygen toward Cu(1) at a longer distance, 2.621(7) Å, and another nitrate oxygen is weakly bound to Cu(2) at 2.760(7) Å (not shown in Figure 1), providing a pseudo-octahedral geometry to the each copper ion with long axial Cu−O bonds as a consequence of Jahn−Teller effect. In **4**, the coordination sphere of the unique copper ion is realized with a similar arrangement as observed for Cu(1) in **1**, but the crystal symmetry leads both the water molecules at the same phenolato side while a nitrate, located on the symmetry plane is bridging the metals on the other side. The Cu−O(1w) and Cu−O(nitrate) distances are sensibly longer, being of 2.581(2) and 2.739(2) Å, respectively. In both the complexes the basal Cu−O distances are comparable in lengths ranging from 1.9136(16) to 1.995(6) Å (Table 3), showing a shorter value for the hydroxido oxygen. On the other hand the Cu−N(imino) bond distance is significantly shorter than that involving the amino nitrogen of the heterocycle ring. The Cu(1)−O(1)−Cu(2) bond angle is of ca. 97.2°, whereas the Cu(1)−O(2)−Cu(2) one, subtended by the hydroxido group is slightly larger, of ca. 100.3°, leading to a metal−metal separation of 2.9794(15) and 2.9435(9) Å in **1** and **4**, respectively. In **1**, the piperazine moieties attain the more stable chair conformation and the uncoordinated amine nitrogens are protonated to provide electrical charge neutrality of the system.

(b) $[Cu(HL1^4)(H_2O)(NO_3)]_2(NO_3)_2\cdot 2H_2O$ (2) and $[Cu(L1^1)(H_2O)(NO_3)]_2$ (3). The crystal structure of **2** and **3** reveals that they comprise dinuclear complex cations, nitrate anions, and water molecules. The complexes are formed by two unsymmetrical tridentate ligands chelating the metal ions and forming a phenoxido-bridged Cu(II) dimer, and both species are located on a crystallographic inversion center. An *ORTEP* view of **3** with atom labeling scheme of the independent part is shown in Figure 3, and a selection of bond lengths and angles is given in Table 4. The metal in both **2** and **3** possesses an octahedral coordination sphere, with two phenoxido-bridged oxygens, an imine nitrogen donor, and a carbonyl oxygen located in the equatorial plane; a water molecule and a nitrate oxygen occupy the axial positions at longer distances. All of the Cu−N and Cu−O bond distances are close comparable ranging from 1.944(4) to 1.955(4) Å in **2**, and from 1.933(4) to 1.952(4) Å in **3**, where the lower values pertains to the Cu−N imino bond, the longer to the Cu−O(phenoxido) one. The axial distances are significantly elongated for the Jahn−Teller effect, the Cu−O(1w) bond length in **2** (2.254(4) Å) is significantly longer than that involving the nitrate (Cu−O(4) 2.622(4) Å), whereas the corresponding values in **3** are comparable being of 2.450(7) and 2.484(10) Å, respectively. The bond angles Cu−O1−Cu′ (101.47(17) and 101.61(18)°), larger than the correspondent values measured in **1** and **4**, lead to an intermetallic separation of 3.0213(13) and 3.0152(15) Å, comparable within their esds. The morpholine moieties,

(35) Lever, A. B. P. *Inorganic Electronic Spectroscopy*; Elsevier: Amsterdam, The Netherlands, 1984; p 553.

Table 3. Selected Coordination Bond Lengths (Angstroms) and Angles (Degrees) for **1** and **4** with Esds in Parentheses[a]

1				4	
Cu(1)−N(1)	1.938(7)	Cu(2)−N(4)	1.939(7)	Cu−N(1)	1.940(2)
Cu(1)−N(2)	2.103(8)	Cu(2)−N(5)	2.104(7)	Cu−N(2)	2.033(2)
Cu(1)−O(1)	1.995(6)	Cu(2)−O(1)	1.971(6)	Cu−O(1)	1.9664(15)
Cu(1)−O(2)	1.946(6)	Cu(2)−O(2)	1.937(6)	Cu−O(2)	1.9136(16)
Cu(1)-O(1w)	2.292(6)	Cu(2)−O(3)	2.404(7)	Cu−O(1w)	2.581(2)
Cu(1)−O(4)	2.621(7)	Cu(2)−O(7)	2.760(7)	Cu−O(3)	2.739(2)
Cu(1)−Cu(2)	2.9794(15)			Cu−Cu′	2.9435(9)
Cu(1)−O(1)−Cu(2)	97.4(3)			Cu−O(1)−Cu′	96.91(10)
Cu(1)−O(2)−Cu(2)	100.2(3)			Cu−O(2)−Cu′	100.55(11)

[a] Symmetry code: primed atoms at $x, -y + {}^1/_2, z$.

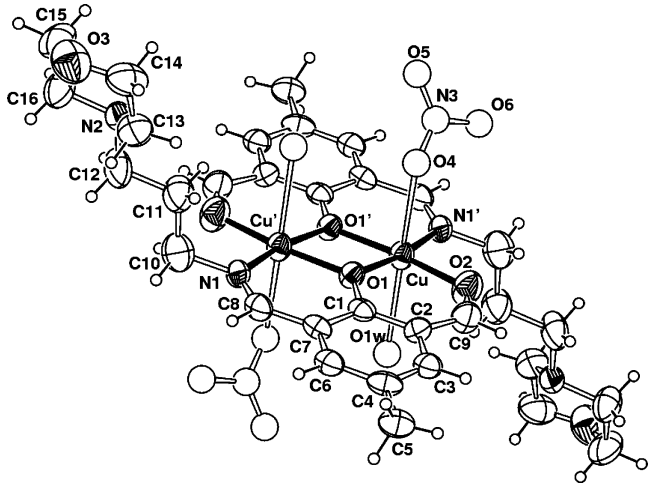

Figure 3. *ORTEP* drawing of **3** with atom labeling (disordered nitrate and aquo ligand indicated as sphere of fixed radius for clarity). The same scheme is applied also to **2** with protonated N(2) atom.

Table 4. Selected Coordination Bond Lengths (Angstroms) and Angles (Degrees) in **2** and **3** with esds in Parentheses[a]

	2	3
Cu−N(1′)	1.944(4)	1.933(4)
Cu−O(2)	1.945(4)	1.936(5)
Cu−O(1)	1.947(4)	1.939(4)
Cu−O(1′)	1.955(4)	1.952(4)
Cu−O(1w)	2.254(4)	2.450(7)
Cu−O(4)	2.622(4)	2.484(10)
Cu−Cu′	3.0213(13)	3.0152(15)
Cu−O(1)−Cu′	101.47(17)	101.61(18)

[a] Symmetry code: primed atoms at $x, -y + {}^1/_2, z$.

which assume the usual chair conformation, are far apart from the metal centers with alkyl chain in antiperiplanar conformation (torsion angles about C−C bond close to 170°). In case of **2**, the morpholine nitrogen atom is protonated to provide electrical charge neutrality of the system.

(c) $[Cu_2(L2^1)(N_3)_3]$ (5). 5 is obtained by adding NaN_3 to a solution of **3**. However the X-ray analysis showed in **5** a different ligand with respect to that present in **3**, which implies that in the presence of azide shuffling of the ligand side arms, via cleavage and reformation of the end-off compartmental species, takes place. The 4-methyl-phenolato ligand coordinates the two metals with the phenoxido bridging oxygen, and the two imine-nitrogen donors, as usually observed in these species. Each copper(II) completes its coordination sphere through azido ligands either as terminal or bridging ligand. Two independent complexes were detected by the X-ray analysis and are shown in Figures 4 and 5. These units

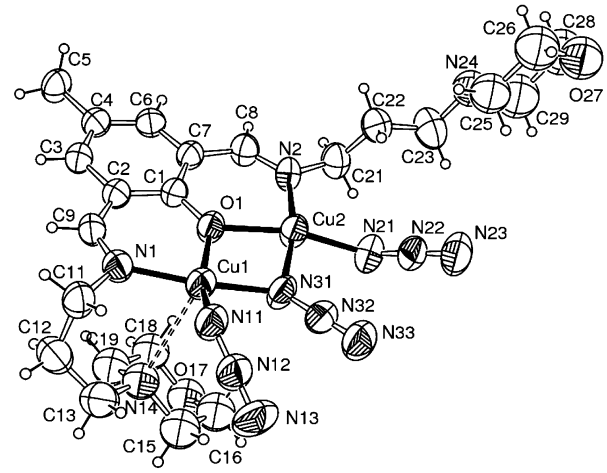

Figure 4. *ORTEP* drawing (40% probability ellipsoids) of complex A of **5** with atom labeling scheme.

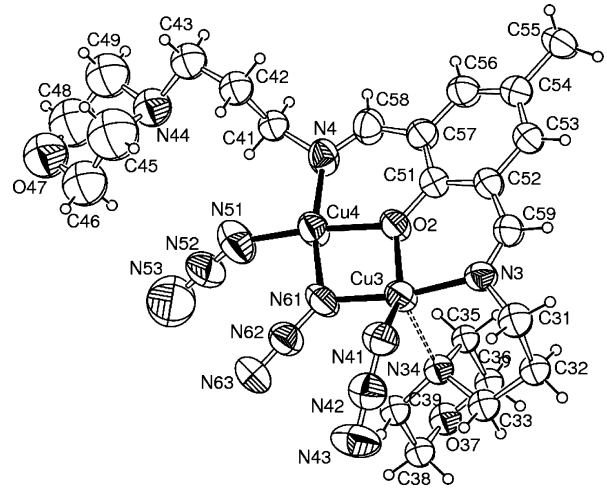

Figure 5. *ORTEP* drawing (40% probability ellipsoids) of complex B of **5**. Both propyl−morpholine units are disordered and only one conformation is shown.

are apparently similar with a morpholine nitrogen acting as donor toward one copper ion [Cu(1) and Cu(3), respectively], but the second complex shows both the propyl−morpholine fragments disordered over two positions (each with 50% ocupancy). The metal ions Cu(1) and Cu(3) have a square-planar geometry, whereas Cu(2) and Cu(4) present a distorted octahedral coordination. Thus, all of the metal ions are coordinated by the phenoxido bridging oxygen, the imine−nitrogen donor and two nitrogen atoms from azide anions, as shown in the pictures. These Cu−N bond lengths are within in a range from to 1.917(8) to 1.993(6) Å, whereas the Cu−O

Table 5. Selected Coordination Bond Lengths (Angstroms) and Angles (Degrees) for **5** with esds in Parentheses

Molecule A			
Cu(1)−N(1)	1.951(5)	Cu(2)−N(2)	1.949(6)
Cu(1)−N(11)	1.981(6)	Cu(2)−N(21)	1.952(6)
Cu(1)−N(31)	1.951(6)	Cu(2)−N(31)	1.973(6)
Cu(1)−O(1)	1.997(4)	Cu(2)−O(1)	2.015(4)
Cu(1)−N(14)	2.821(7)	Cu(2)−N(41)	2.533(6)
Cu(1)−Cu(2)	3.1167(13)	Cu(2)−O(17′)	2.721(6)
Cu(1)−O(1)−Cu(2)	101.93(18)	Cu(1)−N(31)−Cu(2)	105.2(3)
Molecule B			
Cu(3)−N(3)	1.942(5)	Cu(4)−N(4)	1.980(6)
Cu(3)−N(41)	1.993(6)	Cu(4)−N(51)	1.917(8)
Cu(3)−N(61)	1.967(6)	Cu(4)−N(61)	1.978(6)
Cu(3)−O(2)	2.015(4)	Cu(4)−O(2)	2.008(4)
Cu(3)−N(34)	2.278(11)	Cu(4)−O(37″)	2.550(12)
Cu(3)−Cu(4)	3.1490(13)	Cu(4)−N(11)	2.560(7)
Cu(4)−O(2)−Cu(3)	103.01(18)	Cu(3)−N(61)−Cu(4)	105.9(3)

[a] Symmetry code: (′) $-x + {}^{2}/_{3}, -y + {}^{1}/_{3}, -z + {}^{4}/_{3}$, (″) $-x + {}^{2}/_{3}, -y + {}^{1}/_{3}, -z + {}^{1}/_{3}$.

distance appears slightly longer from 1.997(4) to 2.015(4) Å. Cu(1) and Cu(3) complete the coordination sphere with the amino nitrogen of one of the morpholine units, although at a different extent, being the Cu(1)−N(14) bond length of 2.821(7) Å, and Cu(3)−N(34) of 2.278(11) Å. This feature, and the disordered observed in morpholine groups in complex B, indicate that pendant heterocycle rings manifest a great conformational freedom. On the other hand, the axial positions of Cu(2) and Cu(4) are occupied by a N_3 nitrogen and a morpholine oxygen from the other independent complex. These axial Cu−N(azide) distances are comparable in length being Cu(2)−N(41) = 2.533(6) Å, Cu(4)−N(11) = 2.560(7) Å, and this feature forces the correspondent azide to be located outside the mean plane of the phenolato ligand (Figure 2S, Supporting Information). Cu−O(morpholine) is significantly different (Cu(2)−O(17′) = 2.721(6) Å, Cu(4)−O(37″) = 2.550(12) Å). In the crystal these connections form a supramolecular octanuclear entity arranged about an inversion center (Figure 2S, Supporting Information).

Electrochemistry. The cyclic voltammograms of the complexes were recorded in dry acetonitrile medium, and reduction and oxidation potentials for the copper complexes are summarized in Table 6.

All of the complexes exhibit irreversible redox couple. **1** and **4** are associated with the stepwise reduction of the Cu(II) center

$$Cu^{II}Cu^{II} \rightarrow Cu^{I}Cu^{II} \rightarrow Cu^{I}Cu^{I} \quad (1)$$

whereas **2**, **3**, and **5** are associated with one step reduction of the Cu(II) centers

$$Cu^{II}Cu^{II} \rightarrow Cu^{I}Cu^{I} \quad (2)$$

Monitoring of the Reactions of the Dicopper(II) Complex-Catalyzed Oxidation of 3,5-Di-tert-butylcatechol by UV−vis Spectroscopic Study. All of the dinuclear Cu(II) complexes show significant catalytic oxidation activity toward 3,5-di-tert-butylcatechol (3,5-DTBC). This substrate with bulky substituents on the ring has low quinone-catechol reduction potential. This makes it to be easily oxidized to corresponding *o*-quinone, 3,5-DTBQ, which is highly stable and shows maximum absorption at 403 nm in pure acetonitrile (Supporting Information) and 401 nm in methanol.[1] (b) Before proceeding into the detailed kinetic study, we need to check the ability of the Cu(II) complexes to oxidize 3,5-DTBC. For this purpose, 1×10^{-4} mol dm^{-3} solutions of **1**−**5** were treated with 1×10^{-2} mol dm^{-3} (100 equiv) of 3,5-DTBC under aerobic condition. The course of the reaction was followed by UV−vis spectroscopy. The time dependent UV−vis spectral scan was performed in pure acetonitrile (except for **3**, which is sparingly soluble in acetonitrile) as well as in pure methanol.

UV−vis Spectral Study in Acetonitrile. The spectra of **1**, **2**, **4**, and **5** in acetonitrile solution show dramatic changes immediately after addition of 3,5-DTBC. The changes observed in the spectral scan of the four complexes look very similar in the region 200−500 nm and part A of Figure 6 shows the variation of the spectral behavior for **1** as representative of them followed up for 2 h, after the addition of 3,5-DTBC to the acetonitrile solution of **1**. From the figure, it is clear that the band at 371 nm vanishes immediately after addition of 3,5-DTBC, and two new bands are developed at 354 and 448 nm. It is also evident that the band at 448 nm gradually decreases with concomitant increment of the band at 354 nm. Pure

Scheme 3

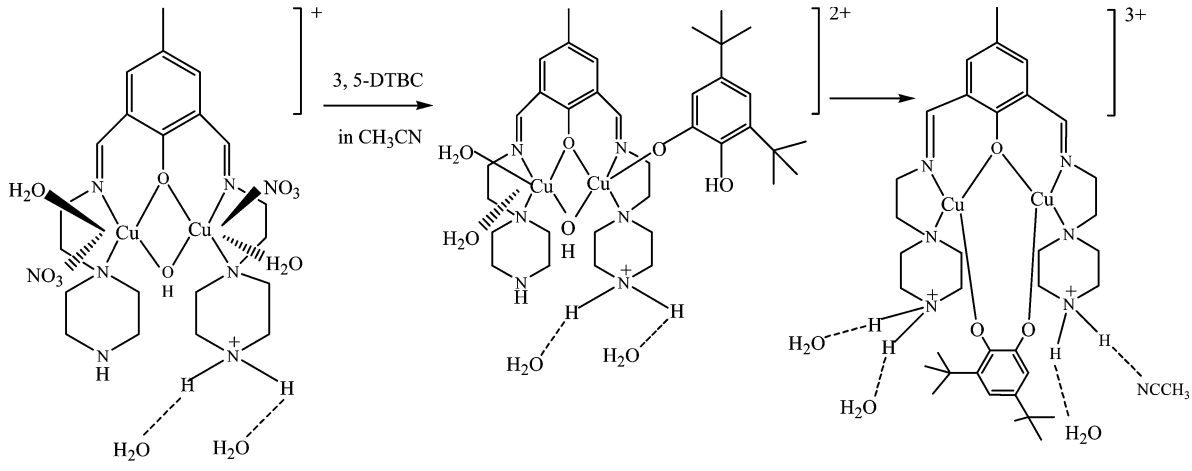

3,5-DTBQ is observed to exhibit band maxima at 403 nm in acetonitrile medium (Supporting Information). Thus, none of the above two band maxima correspond to the formation of 3,5-DTBQ. The spectral scan performed after 4 h from the addition of 3,5-DTBC to the acetonitrile solution of **1** shows that the band maxima at 448 nm nearly vanishes and that at 354 nm attains the maximum peak (part B of Figure 6). The spectral scan performed after 6 h shows the generation of a new band at 401 nm at the cost of the band at 354 nm (part B of Figure 6). We note that the blank experiment (without catalyst) indicates the conversion of 3,5-DTBC to 3,5-DTBQ starts after 12 h under our reaction condition,and therefore we run our catalytic experiment up to 6 h. However, the spectroscopic study suggests that in the presence of these complexes the oxidation of 3,5-DTBC to 3,5-DTBQ takes place via the formation of two intermediates, the enzyme−substrate adducts ES1 and ES2, corresponding to band maxima at 448 and 354 nm for **1** (band positions of ES1 and ES2 for other catalysts are given in the Supporting Information), and the whole process may be represented as follows:

$$E + S \rightarrow ES1 \rightarrow ES2 \rightarrow P + E \qquad (3)$$

where E = complex, S = 3,5-DTBC, and P = 3, 5-DTBQ.

To the best of our knowledge, these sorts of enzyme−substrate adducts have never been characterized previously with 3,5-DTBC as substrate in acetonitrile medium. However, the present investigation unequivocally proves that initially the enzyme−substrate adduct(s) is formed, followed by the oxidation of the substrate by aerial dioxygen in the course of catecholase activity with dicopper complexes. The changes observed in d−d bands during the course of the 2 h reaction are also very remarkable, and part C of Figure 6 represents the changes observed for **1**. The d−d bands of the **1**, **2**, **4**, and **5** are observed to be blue-shifted.

UV−vis Spectral Study in Methanol. The spectrum of **1**−**5** in methanol shows no drastic changes immediately after addition of 3,5-DTBC, in the 200−500 nm region, beside the gradual increment with time of the band ultimately shifted to ∼390nm, that indicates the gradual conversion of 3,5-DTBC to 3,5-DTBQ. Figure 7 shows the changes occurring for **3** as a representative. Here, the most remarkable feature is the absence of the two bands corresponding to the adducts ES1 and ES2, as we observed when acetonitrile is used as solvent. From these data, it should not be excluded the possibility of enzyme−substrate adduct formation prior that substrate oxidation to quinone takes place, but rather that the adduct is too unstable to be detected in methanol medium by the UV−vis spectroscopic method. However, the changes of d−d bands during the 2 h course of reaction indicate a blue shift for **1**, **2**, **4**, and **5** and a red one for **3** and in methanol medium also the d−d bands are retained even after 24 h of reaction, indicating the presence of Cu(II) species.

Table 6. Electrochemical Data for **1**−**5** in Acetonitrile[a]

complex	E^1_{pc}	E^2_{pc}	E^1_{pa}	E^2_{pa}
1	−0.44	−0.76	0.55	−0.03
2	−0.66		0.38	0.01
3	−0.28			0.57
4	−0.31	−0.66	0.49	−0.16
5	−0.54			0.65

[a] V vs SCE. Conditions: Pt working and SCE reference electrodes; supporting electrolyte TEAP; concentration of complexes 1×10^{-3} M, concentration of TEAP 1×10^{-1}M.

It is worth noting that, although the active sites of different forms of catechol oxidase were clearly elucidated by X-ray crystallography, its catalytic mechanism is not fully realized even for the first step of the reaction. Krebs and his group[1,6] proposed a monodentate asymmetric coordination of the substrate, whereas, a simultaneous coordination of the substrate to both copper centers in the bidentate bridging mode was proposed by Solomon and his group.[1] The present study suggests that the oxidation of 3,5-DTBC to 3,5-DTBQ proceeds through the formation of two intermediates, ES1 and ES2. Nevertheless, from the UV−vis spectral study only, no indication on the binding modes of 3,5-DTBC to the copper centers can be guessed. To get a better understanding of the ES1 and ES2 structures, we performed an ESI-MS spectral study by selecting **1** as a catalyst. ESI-MS study of **1** in acetonitrile shows the most abundant peak, called base peak at 725.61 amu, which corroborates well with monopositive species **1a** (*m*/*z*: Calcd 726.71; exptl 725.61 amu) as shown in Scheme 3. Immediately after the addition of 3,5-DTBC to the acetonitrile solution of **1** (complex: 3,5-DTBC = 1:100), the ESI-MS spectrum shows dramatic changes with respect to that of **1.**

The major peaks were observed at 243.24, 301.27, 357.84, 413.44, and 463.47 amu. The ESI-MS spectrum obtained after 2 h of the reaction shows only one main change with respect to that detected after immediate addition of 3,5-DTBC, that is, the formation of a new peak at 276.16 amu with drastic reduction of intensity of the peak at 413.44 amu. The species corresponding to the base peak 413.44 and 276.16 amu may be assigned to **1b** (*m*/*z*: Calcd 412.01; exptl 413.44 amu) and **1c** (*m*/*z*: Calcd 275.33; exptl 276.16 amu), respectively. Though, as shown in Scheme 3, the isotopic distribution patterns for these species do not agree with di- and tripositive charged nature. On the contrary, it is notable that isotopic distribution model of all the peaks corresponds to singly charged species. Thus, it is difficult to come to a definite conclusion regarding the structures of ES1 and ES2 based on ESI-MS technique and extensive further study is underway in our laboratory.

Reactions of the Dicopper(II) Complexes with Tetrachlorocatechol in Acetonitrile Medium Monitored by UV−vis Spectroscopic Study. First of all, the UV−vis activities of pure TCC and pure tetrachloro-*o*-quinone (TCQ) in acetonitrile have been investigated. TCC is observed to be silent in the range of 350−800 nm, whereas TCQ exhibits a band at 437 nm (ε ∼2711 $M^{-1}cm^{-1}$) (Supporting Information). To study the reactions of the dicopper(II) complexes with TCC in acetonitrile medium 5×10^{-5} mol dm^3, solutions of **1**−**5** were treated with 5×10^{-3} mol dm^{-3} (100 equiv) of TCC under aerobic condition. For **2**−**5**, immediately after the addition of TCC to the solution of the complex the

original charge transfer (CT) band vanishes with the formation of a new band at 418 nm for 2, 405 nm for 4 and 415 nm for 5 (Supporting Information). However, in all cases no further change in intensity and band position are observed during 2 h course of reaction when **2**−**5** are used, thus suggesting a mere adduct formation and no oxidation of TCC takes place (as reported by other investigators). But most interestingly when **1** is used as the catalyst, the CT band at ∼370 nm vanishes immediately after addition of TCC with the formation of a new band at ∼410 nm of higher intensity (Figure 8). The time-dependent spectral scan shows that the band intensity increases with time, along with shifting of band maxima which finally moves at 436 nm, and no further change of the band position is observed within a 2 h course of reaction. The band initially formed at ∼410 nm is most certainly TCC → Cu(II) CT in origin and this adduct is observed to generate TCQ as evident from the gradual increment of intensity along with shifting of the band position to 436 nm corresponding to the TCQ species (Supporting Information). To get further experimental evidence to characterize the product we have applied column chromatoghaphic technique to isolate the product in pure form using silica gel column and ethyl acetate−hexane mixture (4:1) as eluent. The isolated species exhibits three equal intensity ^{13}C NMR peaks at 168.95, 143.87, and 132.04 ppm and ν(C═O) stretching frequency at 1679.8 cm^{-1} in its IR spectrum (Supporting Information). The data are perfectly matched with pure TCQ and thereby unequivocally proves the oxidation of TCC to TCQ catalyzed by **1**.

Catechol Oxidase Activity and Kinetics. The kinetics of the 3,5-DTBC oxidation was determined by the initial rates method by monitoring the increase of the product 3,5-DTBQ (at 387 nm for **1**, at 390 nm for **2** and **3**, at 395 nm for **4**, and at 380 nm for **5**). The concentration of the substrate 3,5-DTBC was always kept at least 10 times larger than that of the Cu(II) complex to maintain the pseudo-first-order condition. All of the kinetic experiments were conducted at constant temperature of 20 °C, monitored with a thermostat. Initially, a series of solutions of substrate 3,5-DTBC, having different concentrations (8×10^{-4} mol dm^{-3} — 5×10^{-2} mol dm^{-3}), were prepared from a substrate concentrated stock solution using methanol as solvent. Then, 2 mL of such a substrate solution was poured in a 1 cm quartz cell kept in the spectrophotometer to equilibrate the temperature at 20 °C. A 0.04 mL (2 drops) of 5×10^{-3} mol dm^{-3} of Cu(II) complex in methanol was quickly added and mixed thoroughly so that to get an ultimate Cu(II) complex concentration of 1×10^{-4} mol dm^{-3}. The absorbance was continually monitored at 387 nm for **1**, at 390 nm for **2** and **3**, at 395 nm for **4**, and at 380 nm for **5**. Initial rates were determined from slope of the tangent to the absorbance versus time curve at $t = 0$. Figure 9 represents the dependence of initial rate on the concentration of catechol for the **3** (as a representative). By applying *GraFit32* program for enzymatic kinetics, K_m and V_{max} are calculated from the graphs, and the inset shows the Lineweaver−Burk plot.

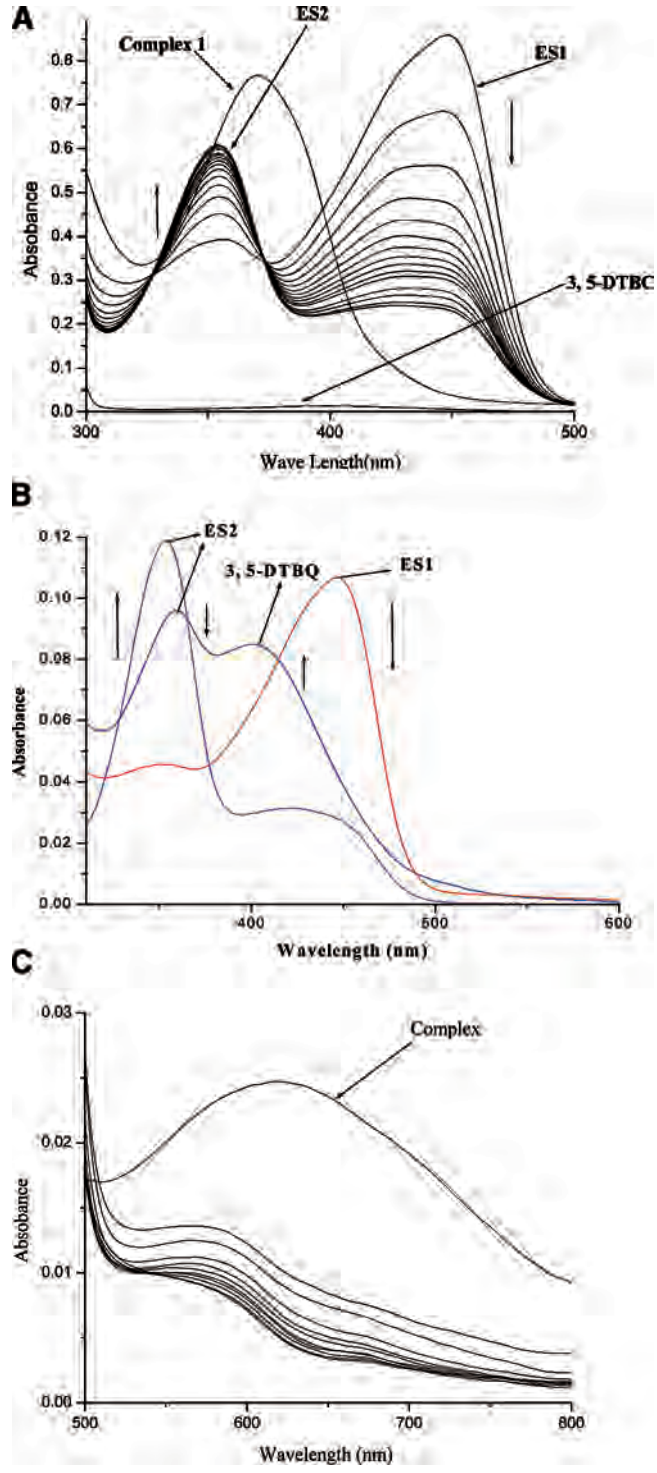

Figure 6. (**A**) UV−vis spectra (300−500 nm) of (i) **1** (conc. 1×10^{-4} M; in CH_3CN); (ii) 3,5-DTBC (1×10^{-2} M in CH_3CN); (iii) changes in UV−vis spectra of **1** upon addition of 100-fold 3,5-DTBC observed after each 10 min interval. (**B**) Changes in UV−vis spectra of **1** upon addition of 100-fold 3,5-DTBC (S) observed: (i) immediately (red); (ii) after 4 h.(black); (iii) after 6 h (blue). (**C**) UV−vis spectra (500−800 nm) of (i) **1** (conc. 1×10^{-4} M; in CH_3CN); (ii) changes in UV−vis spectra of complex **1** upon addition of 100-fold 3,5-DTBC observed after each 10 min interval.

Furthermore, for a particular substrate concentration, varying the Cu(II) complex concentration, a linear relationship for the initial rates was obtained, which shows a first-order dependence on the Cu(II) complex concentration. On

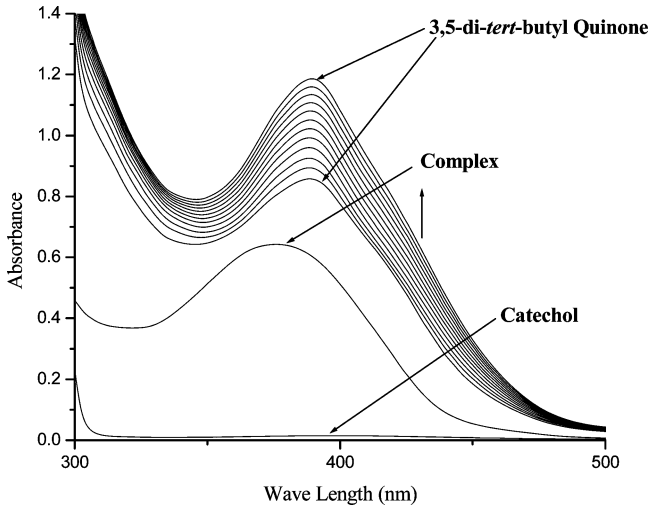

Figure 7. UV−vis spectra (300−500 nm) of (i) complex **3** (conc. 1 × 10^{-4} M; in CH_3OH); (ii) 3,5-DTBC (1 × 10^{-2} M in CH_3OH); (iii) changes in UV−vis spectra of **3** upon addition of 100-fold 3,5-DTBC observed after each 10 min interval.

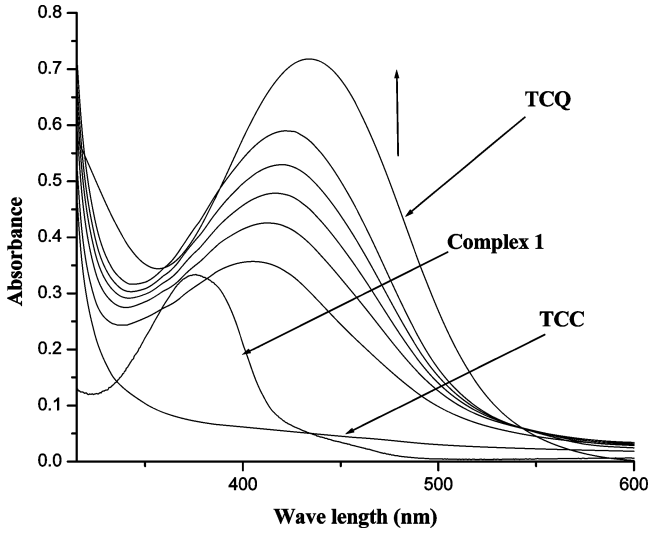

Figure 8. UV−vis spectra (300−500 nm) of (i) **1** (conc. 0.5 × 10^{-4} M; in CH_3CN); (ii) TCC (0.5 × 10^{-2} M in CH3CN); (iii) changes in UV−vis spectra of **1** upon addition of 100-fold TCC observed after each 20 min interval.

the other hand, varying the concentration of 3,5-DTBC, a first-order dependence was observed at low 3,5-DTBC concentration. However, all Cu(II) complexes showed a saturation kinetic at higher 3,5-DTBC concentrations. A treatment on the basis of Michaelis−Menten model was thus seemed to be appropriate. Figure 10 shows the Lineweaver−Burk plots (double reciprocal plot) for the complexes.

From Lineweaver−Burk plots different complex parameters, such as maximum velocity (V_{max}), rate constant for the dissociation of complex-substrate intermediate (i.e., the turnover number, K_{cat}), and Michaelis binding constant (K_M) were evaluated and the data tabulated in Table 7.

Although the real mechanism of the reaction appears rather complicated, the data obtained from Lineweaver−Burk plot are adequate for a catalytic activity assessment. Our complexes demonstrate to be excellent catalyst for conversion of 3,5-DTBC to 3,5-DTBQ. The observed K_{cat} ranges from 1.08 × 10^4 to 3.24 × 10^4 h^{-1}, and the higher value must be

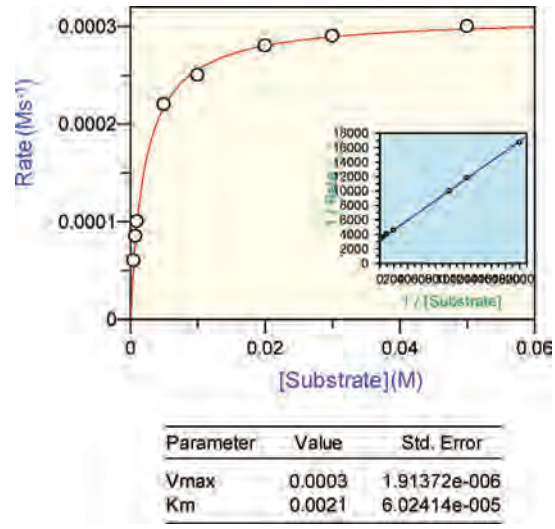

Parameter	Value	Std. Error
Vmax	0.0003	1.91372e-006
Km	0.0021	6.02414e-005

Figure 9. Plot of rate vs concentration of **3.** Plot of inset shows reciprocal Lineweaver−Burk plot for the same complex.

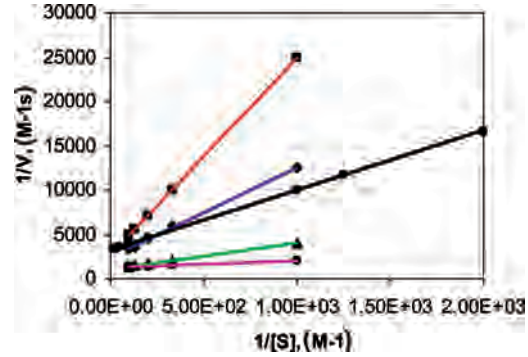

Figure 10. Lineweaver−Burk plots (double reciprocal plot) for the complexes: (green) for **1**, (blue) for **2**, (black) for **3**, (orange) for **4**, and (pink) for **5**.

Table 7. Kinetic Parameters for **1**−**5**

complex	solvent	wavelength (nm)	V_{max} (Ms^{-1})	K_m (M)	K_{cat} (h^{-1})
1	methanol	387	0.0009	0.0023	3.24 × 10^4
2	methanol	390	0.0004	0.0049	1.44 × 10^4
3	methanol	390	0.0003	0.0021	1.08 × 10^4
4	methanol	395	0.0004	0.0076	1.44 × 10^4
5	methanol	380	0.0008	0.0007	2.88 × 10^4

compared with that of ∼1 × 10^4 h^{-1} of the most efficient catalyst reported to date.[20]

Conclusions

Five dinuclear copper(II) complexes have been synthesized with judicious designing of end-off compartmental-type ligand systems maintaining the Cu−Cu separation within the 2.9−3.1 Å range, with the aim to investigate their applicability as structural and functional models to mimic the active site of catechol oxidase. Our investigation establishes that the stability of the enzyme−3,5-DTBC substrate adduct depends on the nature of the solvent and we were capable to characterize spectroscopically in acetonitrile medium the Cu(II)−3,5-DTBC adduct, that is, the initial step of catecholase activity for the first time. In acetonitrile the 3,5-DTBC → 3,5-DTBQ oxidation process catalyzed by our complexes have been observed to proceed via the formation of two enzyme−substrate

adducts, ES1 and ES2. The present complexes exhibit extraordinarily high catecholase activity in methanol medium reducing the gap between the native enzyme activity and its synthetic analogues. **1** exhibits turnover number or K_{cat} of 3.24×10^4 (h^{-1}), which is ~3.5 times higher than the most efficient catalyst reported to date. Moreover, it is also capable to catalyze the oxidation of TCC to TCQ, a reaction never reported with synthesized dicopper complex analogues. Therefore, to the best of our knowledge, the present complexes appear to be the most appropriate structure−functional models to mimic the active site of catechol oxidase.

Acknowledgment. The authors wish to thank the Council of Scientific and Industrial Research, New Delhi (Project No. 01(1871)/03/EMR-II dated 17/03/2003) for financial support.

Supporting Information Available: X-ray crystallographic data in CIF format of **1**−**5**, UV−vis spectroscopic and kinetic data, ORTEP drawing of **2**, and crystal packing of **5**; ESI-MS spectrum for **1** in acetonitrile, and time dependent ESI-MS spectra for **1** and 3,5-DTBC in acetonitrile; CV for **1** and **2**; ^{13}C NMR and IR spectrum for oxidation product of TCC catalyzed by **1**. This material is available free of charge via the Internet at http://pubs.acs.org.

IC701332W